An approach for image-based quantification of fines migration in geologic columns and core samples

Collin R. Sutton[1,*] and *Christopher Zahasky*[1]

[1]University of Wisconsin – Madison, Department of Geoscience, Madison, WI, USA

Abstract. Understanding chemical and colloidal transport processes in conventional and unconventional formations is fundamental to engineering and management of subsurface energy production, carbon capture and sequestration, and hydrogen storage. Migration of variably sized colloids (fines) has been identified as a primary concern for the long-term efficiency of injection and extraction operations in many industry applications. Characterizing the migration of colloids in porous media has been widely studied; however, few studies have quantified sub-core colloidal transport behavior and related this to bulk sample observations. In this study the transport of clay fines through sand packs are analyzed using micro-positron emission tomography (PET) imaging. PET imaging allows for accurate 4-D quantification of clay fines transport at sub-centimeter scale. PET imaging was completed by imaging an aqueous pulse of suspended radiolabeled kaolinite under single-phase flow conditions. This approach allows for the quantification of changes in transport, attachment, and detachment properties at the sub-centimeter scale. Mathematical models were then developed to compare experimental data to the predicted colloidal behavior of the system using a form of the Derjaguin, Landau, Verwey, and Overbeek (DLVO) model to parameterize and interpret solutions of the advection-dispersion-reaction equation. This study provides a novel approach to the quantification of fines migration and colloidal transport behavior in geologic porous media allowing for future work to be done on more complex and heterogenous cores under multiphase flow conditions.

1 Introduction

Colloids in the environmental and energy resources sciences are typically described as being nanometer to micrometer sized insoluble particles of bacteria, viruses, engineered materials, or geologic particulates such as clay [1]. The migration of clay colloidal particles (fines) is of particular interest due to the extensive occurrence of clay minerals throughout all sedimentary basins and during weathering reactions of many common igneous and metamorphic rocks [2]. Kaolinite, illite, smectites, and chlorites are the common clay minerals in sedimentary basins [3]. Understanding the transport and sorption properties of fines are of importance to a variety of geoscience fields such as environmental remediation, water resources management, subsurface energy extraction, geologic storage of carbon dioxide and hydrogen. For example, unconventional wells typically experience a very sharp initial decline in production followed by a slower long-term decline which is usually attributed to formation damage as a result of the migration of fines [4]. The structure, mineralogy, and chemical exchange capacity of clays have been discussed in detail elsewhere [5]. Kaolinite has been identified as a main contributor to formation damage and has been used widely in coreflooding experiments [6,7,8]

Changes in flow and physiochemical conditions are classically considered to be the two primary mechanisms responsible for the attachment or mobilization of fines [1]. Physical attachment mechanisms have commonly been described using colloid filtration theory (CFT) that relates the retention of colloids to the collector and the pore water velocity and can be incorporated into the advection-dispersion equation with first-order kinetics [9, 10]. Changes in physiochemical conditions such as fluid pH and ionic strength are well known to influence the migration behavior of fines and can be characterized by the Derjaguin, Landau, Verwey, and Overbeek (DLVO) model [11, 12]. DLVO theory describes the electrochemical forces acting on a colloid and a collector grain as a result of the chemical conditions of the fluid through the summation of the attractive forces (van der Waals forces) and the repulsive forces (electrical double layer and Born Repulsion). DLVO theory has since had extra processes and forces added and is known as extended-DLVO or non-DLVO forces. These extensions of original DLVO theory are not considered in this study. Electrostatic forces dictate the net repulsive or attractive charges between colloids and collector grains (i.e., porous matrix). Most colloids and collector grains will exhibit negative charges under natural chemical conditions [13, 14]. These net negative charges generate unfavorable colloid attachment conditions due to the net repulsion. However, colloids may be immobilized in the secondary minimum that is controlled by van der Waals forces based on the size of the particles and the separation distance.

The net charge between particles in a system is highly dependent on the pH and ionic strength of the fluid in the system. Ionic strength and pH have been shown to play an important role in the migration potential of fines. High ionic strength of a solution will suppress the electrical double layer of a negatively charged particle due to the high concentration of positively charged cations in solution. This suppression of

* Collin R. Sutton: collin.sutton@wisc.edu

the double layer causes the net charge of the particle to become less negatively charged. Likewise, a lower ionic strength solution will cause the electrical double layer to expand and cause the particle to have a more negative charge. As a result, a lower ionic strength solution is expected to cause more migration of fines in a reservoir [15].

In addition to ionic strength, there is a pH-dependent process by which fines have a larger migration potential. Acidic conditions lead to a lower fines migration potential than basic conditions [16]. The reason for this relationship is that by definition more H^+ ions are present in acidic solutions and will keep the surface potential of the clay low resulting in more positive zeta potentials. As the pH increases, OH^- becomes increasingly dominant and will increase the surface potential or cause more highly negative zeta potentials. This logic is supported by literature that shows that acidic environments lead to stable permeability while transitions to basic environments lead to loss of permeability in the formation [6,17]. The isoelectric point, also called the point of zero charge, typically exists between the extreme acidic and basic ranges for colloids. Kaolinite, and clays in general, have a complex chemical structure and the exact isoelectric point can be difficult to determine if one exists at all. Many studies have been conducted and point to a range of possible isoelectric points ranging from below a pH of 3, a pH of between 4 and 7, and none [18,19,20,21]. Overall, formations with more basic pH and lower ionic strength will lead to increased fines migration while more acidic and higher ionic strengths will lead to more stable fines [14,16].

Classical versions of CFT and DLVO theory alone have been shown in literature to not sufficiently summarize the behavior of fines in natural systems [22]. Therefore, the colloidal system is likely controlled by a combination of hydrodynamic and physiochemical properties which need to be combined to better understand the transport phenomena. The aim of this study is to combine modeling techniques with coreflooding experiments to determine the feasibility of using a CFT and DLVO based method to predict fines migration under different ionic strength conditions at a stable pH. A 1-dimensional analytical model is used to model expected kaolinite fines migration behavior based on the advection-dispersion equation with first order attachment. DLVO modeling is done for a kaolinite-quartz system to determine net force charges for the system based on varying ionic strength conditions. Core flooding under brackish and freshwater conditions is conducted and quantified using a UV-Vis spectrophotometer. A novel micro-positron emission tomography (micro-PET) approach and dataset is presented. Spectrophotometry and micro-PET are used to measure the attachment and mobilization of kaolinite fines in response to a transition from high to low salinity fluid injection in sand pack experiments.

2 Methodology

Coreflooding experiments are carried out by performing pulse-type experiments in homogenous sand packed columns. The first method involves using a conservative fluorescent tracer and then a pulse of kaolinite measured downstream of the column through a UV-Vis spectrophotometer. The second method involves using micro-PET to image a conservative radiotracer and then radiolabeled kaolinite in four-dimensions.

2.1. Materials

Stock solutions of brackish water with a concentration of 100 milliMolar (mM) NaCl and slightly saline freshwater with a concentration of 1 mM were prepared for use in the coreflooding experiments. Deionized water was used for mixing all solutions. The pH of all solutions were buffered using Piperazine-1,4-bis (2-ethanesulfonic acid) sesquisodium salt (PIPES) with a molarity of 100 mM. PIPES was chosen to minimize complexation and competitive sorption with heavy metals and buffering capacity from pH of 6.1-7.4 [23]. PIPES was dissolved in 100 mM NaOH before being mixed with DI water and a final pH of 7.0 was obtained by further titration with NaOH.

Kaolinite clay was chosen as the colloid for the experimental study due to being an abundant, naturally occurring clay mineral and has very little capacity for swelling [2]. A kaolinite solution of 150 mM kaolinite was selected and stock solutions of kaolinite in 100 mM NaCl with 100 mM PIPES buffer and kaolinite in 1 mM NaCl with 100mM PIPES buffer were made and agitated for a period of 24 hours on a rotating stirrer. A 150 mM kaolinite solution was determined based from radiolabeling batch-type experiments and will be explained in the following sections.

A relatively homogenous, pure quartz sand was used for the column experiments. Ottawa sand was purchased from ThermoFisher Scientific and sieved to 355-500 micrometers in size. The sand was fired for a period of 24 hours at 550 degrees Celsius to remove any residual organic matter.

2.2 Radiolabeling of Kaolinite with ^{64}Cu

$^{64}Copper^{2+}$ ($^{64}Cu^{2+}$) was chosen as the positron emitting radioisotope for this study due to the well-established sorption capacity of copper to kaolinite [24, 25, 26] and has a half-life of 12.7 hours. These studies have also shown that copper has a strong sorption capacity as pH of the solution increases and as ionic strength decreases. Copper also has a very fast equilibration time with clays which is ideal for radiolabeling and imaging due to the time dependency of radioactive decay [26]. A PIPES buffer was used in all radiolabeling experiments as a result of this pH dependency. Furthermore, $^{64}Copper$ is well studied and used in the medical physics literature with PET imaging [27, 28].

Batch-type experiments were conducted with $^{64}Cu^{2+}$ to validate the literature results and to verify that copper would not desorb during the PET experiment. $^{64}Copper^{2+}$ was obtained from the University of Wisconsin-Madison Cyclotron group as 10µL of $^{64}CuCl_2$ + 0.5M HCl. Batch-type experiments were conducted [29] to quantify Cu sorption to kaolinite over multiple orders of magnitude ranges of molarity at different ionic strengths from 0.1M NaCl to DI water. A dose of 1-2 mCi/mL has been found to be the ideal range of radioactivity in the micro-PET scanner for geologic media [30]. The amount of sorbed versus aqueous $^{64}Cu^{2+}$ was determined by taking bulk samples of radiolabeled kaolinite and solution and comparing those against supernatant from centrifuged radiolabeled kaolinite. Desorption experiments

were conducted by removing all supernatant and resuspending the radiolabeled kaolinite in non-radiolabeled solution. Radioisotope concentrations in bulk solutions and supernatant were measured using a Perkin Elmer Wizard2 Gamma Counter.

2.3 Column Experiments

Homogenous sand columns are used to test the transport and flow behavior of fluorescein and kaolinite clay. Fluorescein is chosen because it is considered to be a conservative tracer in low organic content porous media, and it is easily measured with a UV-Vis spectrophotometer. Kaolinite with a concentration of 150 mM is used for all column experiments based on results of the radiolabeling batch-type experiments explained in the previous section. A serial dilution of kaolinite solutions analysis was performed to identify the linear range of absorbance that may occur in the molarity ranges around 150 mM. A linear trend of molarity to absorbance is needed to allow for a linear regression to be performed to calculate concentration of kaolinite in effluent. Total concentration of kaolinite (in molarity) can then be determined by integrating the total volume of the absorbance breakthrough curve. The dilution analysis is performed by making a kaolinite solution at 250 mM by mixing 3.2g of kaolinite in 10 mL of DI water. Multiple subsets of the solution are diluted in half multiple times to achieve a range of concentrations from 250 mM to 0.977 mM. These samples are then analyzed on a Shimazu 1900i UV-Viz spectrophotometer to determine absorbance values over a range of kaolinite molarities.

The column used for the experiment is 1-inch in diameter and made of polyetheretherketone (PEEK). PEEK is used for the column design due to having a high tensile strength and does not interfere with imaging systems such as micro-positron emission tomography or x-ray computed tomography. The column is approximately 11.9 cm long with two cylinder caps made of aluminum with a total length of 3.175 cm each. These caps screw into the PEEK and provide a seal at both ends of the column. A 150 mesh filter is placed in the column and then it is wet packed with sand on a vortex mixer to ensure consistent packing with no air gaps.

The column experiments are performed from an experimental cart system (Figure 1) that was designed to be used with varying geologic materials, at varying confining pressures, over a range of temperatures. This system can be transported to different imaging facilities for imaging while running a column experiment. The system uses a Vindum 3.5K water pump to inject water at a constant flow rate into an inlet port on the column. The inlet and outlet caps are designed with a cross pattern and concentric rings to limit the effects of point-source flow. The water is then pumped at 1 mL/min through the sand core until water leaves the effluent port and then enters a flowthrough quartz cuvette in the UV-Vis spectrophotometer. A differential pressure transducer is connected to the side ports of the inlet and effluent caps to monitor differential pressure throughout the experiments.

Columns are saturated for a minimum of 10 pore volumes with DI water before any injection of solute. A 1 mL pulse is measured by using a pre-cut 1 mL coil of tubing that is attached to a Harvard syringe pump and the Vindum pump through a 6-port Vici valve. First, a 1 mL pulse of the conservative tracer fluorescein is injected into the column at a rate of 1 mL per minute to determine solute advection and dispersivity in the sand pack and to ensure there are no flaws in the column packing. Next, a 1 mL pulse of 150 mM kaolinite is injected and is measured by the UV-Vis spectrophotometer. A second experiment was repeated for 100 mM NaCl + 100 mM PIPES as the saturating fluid and the fluid in the kaolinite suspension. The saturating fluid was injected until no more kaolinite was recorded by the UV-Vis and then the injection fluid was changed to 1 mM NaCl+ 100 mM PIPES at a flow rate of 1.8 mL per minute to determine remobilization behavior of kaolinite as a response to changing ionic strength.

2.4 Transport Model

The advection-dispersion equation (ADE) is used to model kaolinite moving through a sand pack. A modified version of the ADE is used to account for first-order kinetics that describe the attachment and detachment behavior of colloids. The ADE and ADE with reactions can be described as:

$$\frac{\partial C}{\partial t} = D\nabla^2 C - v\nabla C \quad (1)$$

Where C is concentration [mol/L], t is time [s], v is the pore water velocity [m/s], D is the dispersion coefficient [$\frac{m^2}{s}$], $D = D_e + \alpha_L v$, where D_e is the diffusion coefficient and α_L is the longitudinal advection [m]. This equation can then be modified to add a first order reaction term based off the differential rate law, $\frac{\partial C_a}{\partial t} = -kC_a$, where some amount of colloids will attach over the transport distance.

$$\frac{\partial C_a}{\partial t} = D\frac{\partial^2 C_a}{\partial x^2} - v\frac{\partial C_a}{\partial x} - kC_a \quad (2)$$

Where C_a is the solute or colloid concentration and k is the first order attachment or detachment coefficient depending on the sign. This approach is especially useful for column experiments with colloidal transport because van Genuchten and Alves [31] have published 1D analytical solutions that solve these flow equations. This analytical solution is written in python to solve mathematically. It is solved with type 1 flux average boundary conditions [32] specifically, $C(x = 0, t) = C_0 \quad 0 < t \leq t_0$ and $C(x = 0, t) = 0 \quad t \geq t_0$. The ADE with first order reaction can then be further used to describe colloid transport because kC_a can be estimated by using colloid filtration theory (CFT) and is described by Yao et al. [9]. The total of the forces described by CFT can be summed as η and then can be used in an attachment coefficient term from Li et al. [33] to describe the colloidal behavior:

$$k = \frac{3}{2}\frac{(1-\phi)}{d_c} v\alpha\eta \quad (3)$$

Where ϕ is porosity, d_c is the diameter of the collector grain [m], and α is the attachment term. The particle size of a kaolinite grain was assumed to be around 1 μm.

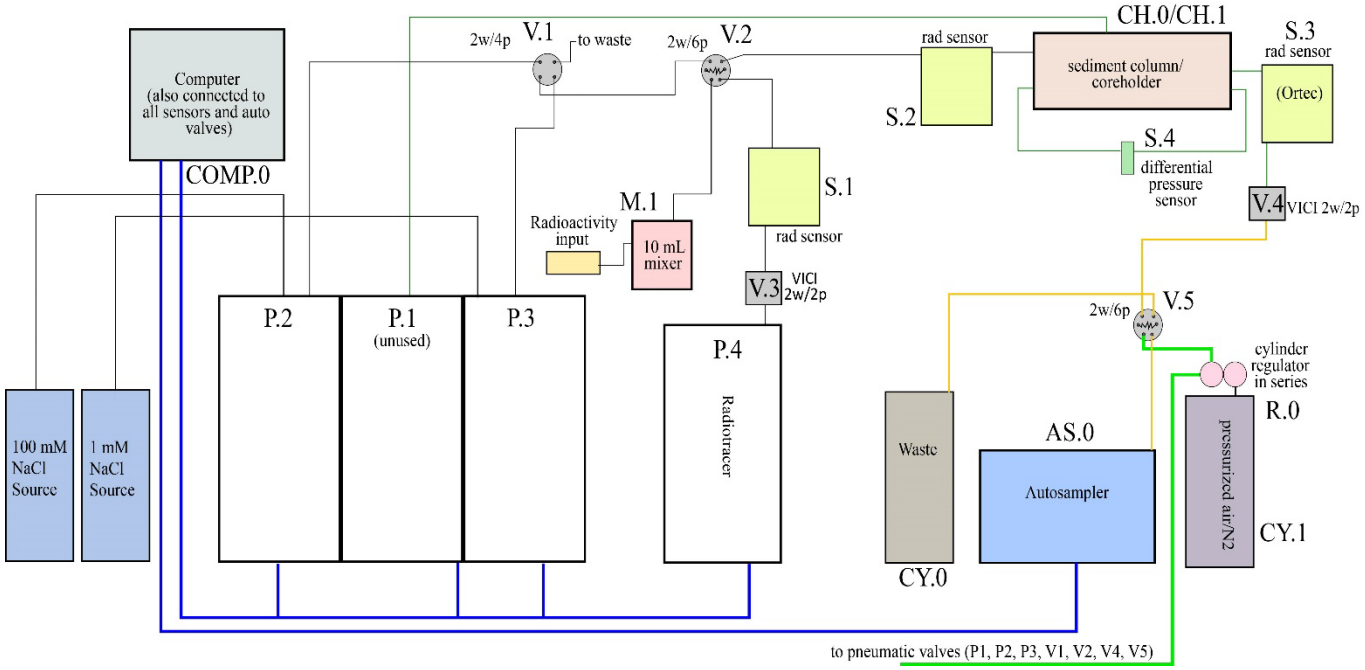

Fig. 1. Schematic diagram of the experimental system for column experiments. Saline solutions were pumped from the source using P.2 and P.3 and were alternated by using V.1. Kaolinite, fluorescein, and radiotracer was loaded and injected by using P.4 and V.2. Radiotracer and radiolabeled kaolinite were monitored in the influent and effluent ends of the column by using S.1, S.2, and S.3 . S.4 is the differential pressure sensor and was used to monitor the pressure in the column throughout the experiment. Sample is sampled using a modified Opentrons OT-One sampling system. All gas lines and pneumatic valves are operated using nitrogen gas.

2.5 Derjaguin, Landau, Verwey, and Overbeek model

The DLVO model is used to determine the total repulsive and attractive forces between a colloid and a collector grain [11, 12]. The method used in this study has been sufficiently discussed elsewhere and a detailed description of the methodology and equations can be found [14, 34]. In general, the DLVO model can be characterized as:

$$V_{DLVO} = V_{LDW} + V_{EDL} + V_{BR} \quad (4)$$

Where V_{DLVO} is the total summation of the forces, V_{LDW} is the van der Waals forces, V_{EDL} is the electrical double later force, and V_{BR} is the Born repulsion force. DLVO forces are controlled by the ionic strength of a solution and the zeta potential of the colloid and the surface grains in the system. Zeta potentials were measured at the University of Wisconsin–Madison Wisconsin Centers for Nanoscale Technology laboratory with a Malvern Zetasizer Nano ZSP. Zeta potentials were measured for kaolinite over a range of pH conditions from 2-10 and over a range of NaCl conditions from 3M to 1mM. Zeta potentials for Ottawa sand were taken from literature [35].

2.6 Micro-Positron Emission Tomography

Micro-Positron Emission Tomography has recently begun to be used as an imaging technique for geologic media [30, 36, 37]. Micro-PET utilizes a 3-D array of photon detectors to simultaneously track photon coincident events across the entire volume of PET scanning field of view. This method allows for a 3-D image reconstruction of a radioisotope distribution through time within a sample. A detailed description of the method and it's use with geologic porous media can be found elsewhere [30]. All micro-PET experiments were conducted at the University of Wisconsin Small Animal Imaging & Radiotherapy Facility using a Siemens Inveion hybrid micro-PET/CT scanner with a 1.2 mm resolution and 13 cm axial field of view. The reconstruction of micro-PET images gives a spatial resolution of 0.077 cm x 0.077 cm x 0.08 cm for each 3D reconstruction within the column.

All experiments are conducted using the same experimental setup as the previous section. The primary differences between the column experiments described above and the micro-PET experiments is that the UV-Vis Spectrophotometer is no longer used in the micro-PET experiments and the kaolinite is radiolabeled with ^{64}Cu to be detected by the micro-PET imaging. ^{18}F radionuclide attached to Fludeoxyglucose ($[^{18}F]FDG$) is used as a conservative tracer and $^{64}Cu^{2+}$ is used as the radiolabel for kaolinite.

Three trials are conducted as a part of the micro-PET imaging experiment. The sand pack is saturated with a minimum of 10 pore volumes of 100 mM NaCl + 100mM PIPES solution before experiments begin. 100 mM NaCl solution is injected constantly at a rate of 1 mL/min and 1 mM NaCl is injected at 1.8 mL/min. All pulses of tracer and kaolinite are prepared in a solution of 100 mM NaCl and 100mM PIPES to maintain ionic strength and pH. First, a 1 mL pulse of $[^{18}F]FDG$ is injected into the homogenous sand pack to determine the ideal transport behavior of the sand pack. Second, a 1mL pulse of $^{64}Cu^{2+}$ radiolabeled 150 mM kaolinite is injected into the column and imaged. Lastly, the injecting solution is switched to a 1 mM NaCl + 100 mM PIPES solution to simulate low salinity injection. A modified Opentrons OT-One Robot Pipetting autosampler is used during radiolabeled injection to verify that effluent is radiolabeled clay fines and not free $^{64}Cu^{2+}$ in solution.

3 $^{64}Cu^{2+}$ and Kaolinite Radiolabeling

Radiolabeling experiments were conducted according to the method described in the above radiolabeling section to ensure that ^{64}Cu imaged with micro-PET was fully sorbed to the kaolinite and not in solution. Results of radiolabeling indicate that $^{64}Cu^{2+}$ has a strong affinity to sorb with kaolinite under all ionic strengths tested for this study. A higher concentration of kaolinite in solution was determined to correspond to a higher percentage of $^{64}Cu^{2+}$ sorbed versus $^{64}Cu^{2+}$ in aqueous phase. An initial concentration of 150 mM kaolinite in DI water had ~2% of initial $^{64}Cu^{2+}$ remaining in aqueous phase after centrifugation. Higher ionic strength solutions led to less sorption of $^{64}Cu^{2+}$ but minimally so. Ionic strengths of 100mM NaCl and 1 mM NaCl had ~10% and ~7% of initial $^{64}Cu^{2+}$ remaining in aqueous phase after centrifugation respectively. Lastly, a wash was done to determine the effects of introducing radiolabeled kaolinite to a dilute solution without radiolabel present. Kaolinite suspensions were washed with the same solution that they were initially suspended in (e.g., 150mM kaolinite suspended in DI water was washed with DI water and so on). Supernatant of washed samples was determined to contain 1-2% of initial $^{64}Cu^{2+}$ leftover in aqueous phase after centrifugation. This 1-2% was likely due to imperfect separation of centrifuged kaolinite and original supernatant with some residual amounts of $^{64}Cu^{2+}$ in the sample tubes.

4 Tracer and kaolinite pulse injection with UV-Vis Spectrophotometry

Columns were packed and ran for different ionic strengths to test the hypothesis that ionic strength plays a key role in the attachment and remobilization of kaolinite and to understand potential hysteresis in the attachment and remobilization processes. A tracer of fluorescein was injected into each column (Figure 2) to determine column integrity (i.e., there are no preferential flow paths or residually trapped air) and could be used to determine longitudinal dispersivity for the transport model. The column experiments at different ionic strengths show results that match the theoretically expected results (Figure 2). Column pressure is monitored with a differential pressure sensor (Figure 1). No pressure discrepancies were observed during any injection experiment. The column with initial lower ionic strength (DI water) has more kaolinite in the effluent than does the column with higher initial ionic strength (100 mM NaCl). Both injections appear to stabilize over time with no additional kaolinite flowing through the system. This implies that all remaining kaolinite in the column is attached to sand or has been trapped in pore throats. Kaolinite is remobilized and again seen in the effluent when the 100 mM NaCl solution is transitioned to 1 mM NaCl injection solution (Figure 3). Therefore, lowering the ionic strength of the system also appears to play a role in the detachment or remobilization of kaolinite.

Kaolinite molarity in the effluent was calculated based on the method developed from the dilution analysis. Normalized curves of kaolinite breakthrough could then be plotted (Figure 2). This allows for quantification of total mass of kaolinite that was transported through the column and total mass that was retained inside the column. The DI water column had a total kaolinite effluent mass of 0.73 mM kaolinite (0.5% of the initial mass) and the high saline column had a total kaolinite effluent of 0.12 mM kaolinite (0.08%). This also validates that high ionic strength leads to stronger attachment of kaolinite than does lower ionic strength. The total mass of kaolinite initially transported and also remobilized during the high to low saline injection transition experiment was 0.42 mM kaolinite (0.28%). This is an increase of 0.3 mM in effluent from decreasing the ionic strength and increasing flow rate of the injection solution. These results indicate that the initial attachment of kaolinite likely has little effect on the stability of colloid attachment.

5 Transport and Electrochemical Modeling

Analytical modeling using the ADE with first-order reactions and CFT was calculated to determine analytical fit to experimental data. First, a tracer data set was used to help fit the longitudinal dispersivity of the analytical solution. The analytical solution fits the experimental breakthrough curve very well (Figure 4). The experimental tracer arrives slightly later and displays slightly more dispersion than does the analytical solution, but this is expected considering fluorescein will show some dispersion in the tubing of the system.

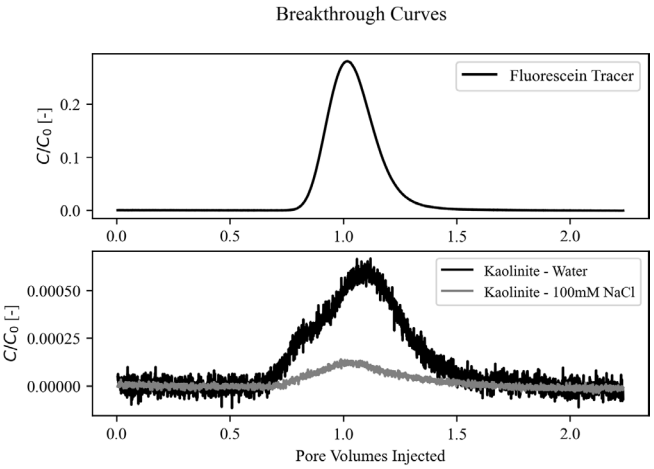

Fig. 2. Top) Normalized breakthrough curve of conservative fluorescein injected into Ottawa sand column that had been saturated with DI water. Bottom) Normalized breakthrough curves of 150mM kaolinite suspended in DI water injected into Ottawa sand column that had been saturated with DI water (black curve with higher peak) and 150mM kaolinite suspended in 100mM NaCl injected into Ottawa sand column that had been saturated with 100mM NaCl (grey curve with lower peak). The pH of all solutions is at a pH of 7. Both plots are plotted as a function of pore volumes injected.

Kaolinite transport can then be modelled using a combination of the ADE with reactions and CFT. Results from the modelled vs experimental kaolinite column experiments can be found in Figure 3. The attachment term, k, can be found in equation 5 and is controlled in part by a fitting parameter, (α). Values for α used in the modeled results indicate that higher saline solutions create a more favorable environment for kaolinite attachment onto collector grains than does lower saline or DI water solutions. This

agrees with the raw data from the column experiments and from published literature [10].

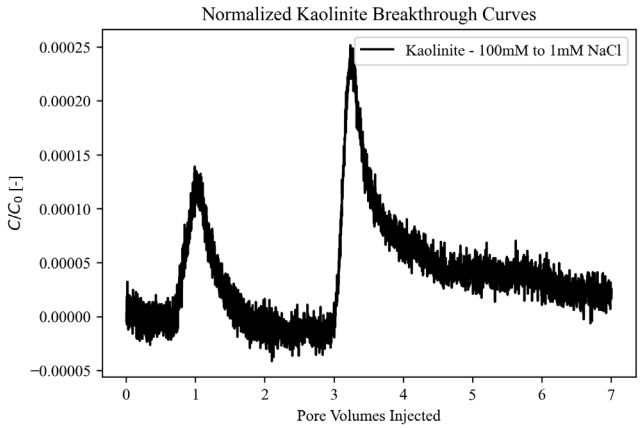

Fig. 3. Normalized breakthrough curve of 150mM kaolinite suspended in 100mM NaCl injected into Ottawa sand column that had been saturated with a 100mM NaCl solution (pH=7). Injection fluid salinity was changed to 1mM NaCl when pore volumes injected was 2.17 (40 minutes).

Modelled results for the kaolinite experiments match very well with the column experiment data. Concentration measurements of kaolinite in effluent resemble experimental data trends closely. Estimates of kaolinite transported through the column were 0.45 mM kaolinite by the analytical solution while the experimental data was 0.73 mM. The saline water analytical model estimated 0.07 mM kaolinite in the effluent while the experimental data was 0.1 mM. Lastly, the curves of the analytical breakthrough are very similar in peak height but tend to peak earlier than the experimental data with less tailing. The experimental kaolinite curves also tend to breakthrough earlier at low ionic strength.

Results of DLVO modeling match published literature and show that a system with kaolinite and quartz sand should be expected to have a deep well of primary attraction at very close separation distances (<1 nm) and higher ionic strengths with a very small or nonexistent energy barrier [9, 24]. The primary attraction decreases with decreasing ionic strength and a larger energy barrier is formed pushing the secondary minimum further from the surface of the collector grain. At further distances, the kaolinite is less likely to be trapped and explains the increase in transport at lower ionic strengths and why the transition from 100mM NaCl to 1mM NaCl remobilizes the previously attached kaolinite

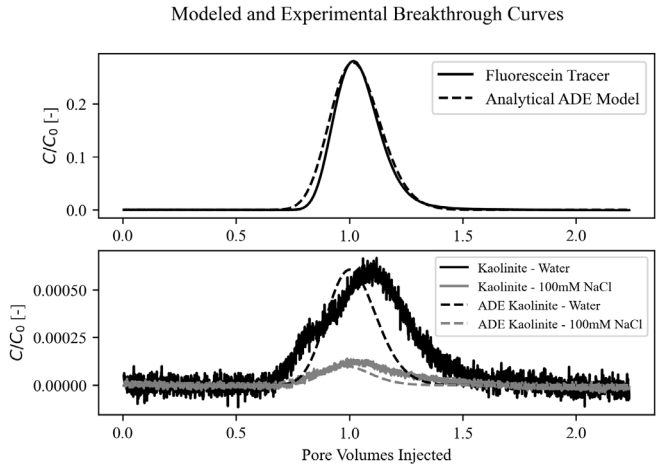

Fig. 4. Top) Normalized experimental tracer from column experiment (solid black) and the analytically modelled tracer (dashed black) from the ADE with reaction solution from Parker and van Genuchten [22]. Bottom) Normalized breakthrough curves of 150mM kaolinite suspended in DI water injected into Ottawa sand column that had been saturated with DI water (black curve with higher peak), analytically derived breakthrough curve (dashed black), 150mM kaolinite suspended in 100mM NaCl injected into Ottawa sand column that had been saturated with 100mM NaCl (grey curve with lower peak), and analytically derived breakthrough curve (dashed gray).

6 Micro-Positron Emission Tomography Imaging

Micro-PET imaging was performed on three sets of experiments: a tracer pulse of [^{18}F]FDG, a pulse of $^{64}Cu^{2+}$ radiolabeled 150mM kaolinite in a sand pack saturated with 100mM NaCl, and a transition from 100mM NaCl to 1mM NaCl to simulate low saline injection. The results of the tracer pulse are reported in Figure 5 and shows normalized tracer concentration as a function of distance from the column inlet at several different pore volumes injected. Next, a radiolabeled pulse of kaolinite is injected into the sand pack and the results are reported in Figure 6. Lastly, a transition from 100mM NaCl to 1mM NaCl injection fluid is reported in Figure 7.

The saline injection of kaolinite (Figure 6) is exceptionally different than the tracer pulse in Figure 5. The radiolabeled clay penetrates the column to a maximum depth of around 2 cm before it is completely attached and immobilized. Autosampling of effluent and radiation probes at the effluent side of the column also validate this observation that kaolinite was immobilized in the column. Transitioning from 100mM NaCl injection solution to 1mM injection solution should theoretically remobilize the kaolinite and move it through the column. However, we do not see remobilization of kaolinite in response to changes in ionic strength (Figure 7). There may be very slight movement throughout the injection period, but this movement is extremely minor and likely only fractions of a centimeter.

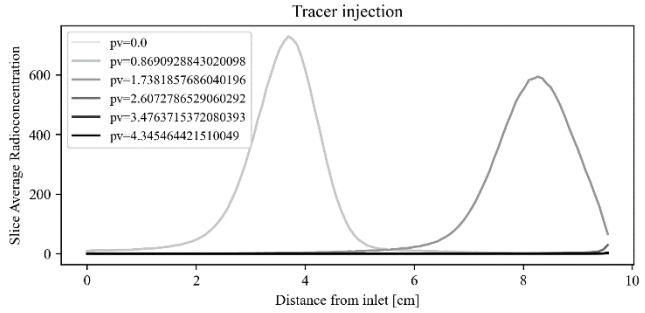

Fig. 5. Normalized [^{18}F]FDG tracer pulse concentration profiles through a homogenous Ottawa sand pack as a function of column length. Concentration profiles are plotted as a summation of radioconcentration as a function of pore volumes injected.

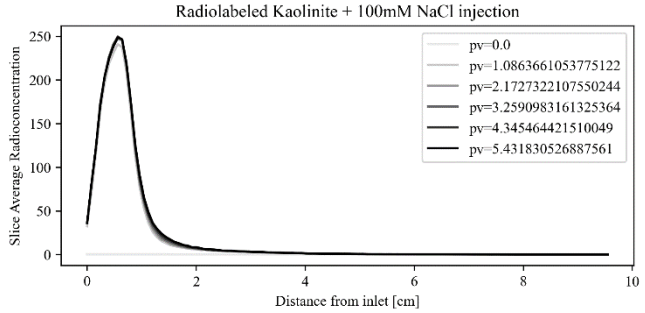

Fig. 6. Normalized $^{64}Cu^{2+}$ radiolabeled kaolinite in 100mM NaCl concentration profiles through a homogenous Ottawa sand pack as a function of column length. This plot shows the injection of kaolinite into the sand pack. Pore volume 0 is seen on the bottom of the plot since no radioisotope has been imaged yet. Breakthrough is plotted as a summation of radioconcentration as a function of pore volumes injected.

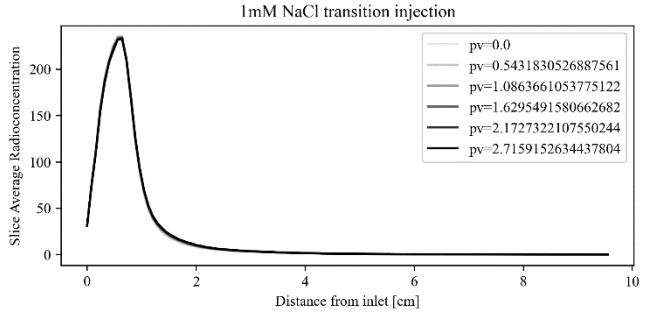

Fig. 7. Transition from $^{64}Cu^{2+}$ radiolabeled kaolinite in 100mM NaCl solution to a 1mM NaCl solution saturating the homogenous Ottawa sand pack column as a function of column length. This plot shows the transition from higher to lower ionic strength, so pore volume 0 is seen on the top of the plot of the plot since radiolabeled kaolinite was in the column when the PET scan began. Concentration profiles are plotted as a summation of radioconcentration at different pore volumes injected.

7 Discussion and Conclusion

Coreflooding experimental data with the UV-Vis spectrophotometer showed kaolinite is transported through the sand packs under all ionic strength conditions. Low ionic strength solutions showed higher tendency for kaolinite transport and less attachment to sand grains. Higher ionic strength solutions displayed higher tendency of kaolinite attachment and less transport through the sand packs. Transitioning from higher to lower ionic strength follows this trend and results in an increase of kaolinite in the effluent even when kaolinite appears to be immobile under the higher ionic strength condition.

Analytical methods agreed with these observations. Analytical solutions to the 1D ADE with first-order reactions paired with colloid filtration theory give rough approximations of kaolinite transport and accurately can predict the order of magnitude of transport. This method does have limitations, however. The analytical solution does not account for the strong tailing behavior of kaolinite, nor does it account for faster than expected arrival times. There is also no way to account for the second peak that happens as a result of transitioning from 100mM NaCl to 1mM NaCl. DLVO calculations provide valuable context for electrochemical conditions of attachment or repulsion in the system and accurately predict the favorability of colloid transport or retention under NaCl and DI water saturating phase conditions.

Micro-PET experiments showed results that differ drastically from the non-radiolabeled column experiments and the analytical solutions. The [^{18}F]FDG radiotracer experiment behaved exactly as expected and was similar to fluorescein experiments in terms of timing and transport. The $^{64}Cu^{2+}$ radiolabeled kaolinite displayed transport behavior that was unlike the non-radiolabeled kaolinite in the UV-Vis spectrophotometer. Radiolabeled kaolinite traveled only a few centimeters into the sand pack columns and was completely immobilized. Transitioning from a high ionic strength solution to a low ionic strength solution resulted in essentially no remobilization and transport of kaolinite.

It is likely that the sorption of $^{64}Cu^{2+}$ to kaolinite leads to drastic changes in the surface charge of kaolinite based on the results of the micro-PET imaging experiments. Al-Sarihi et al. [38] present one of the only studies on this topic and identify that $CaCl_2$ (a divalent cation) leads to no fines migration while NaCl (a monovalent cation) leads to fines migration. This study validates that a monovalent cation alone (NaCl) will lead to migration even at higher ionic strengths while a divalent cation ($^{64}Cu^{2+}$) will lead to immobilization. However, the previously mentioned study found that clays with Ca^{2+} sorbed will remobilize when the saturating solution is transitioned to a solution with monovalent cations. This effect was not seen in our study, and it is likely that different types of divalent will behave differently. It is also unlikely that the $^{64}Cu^{2+}$ imaged during the PET scan desorbed and attached to the porous medium rather than the kaolinite due to the lack of desorption seen during batch desorption experiments.

Kaolinite transport, immobilization, and remobilization behavior may heavily rely on the available cations in the system and the flushing solution. This study is a step towards showing that electrochemically driven fines migration is a highly coupled process that is not controlled solely by ionic strength, but also by available cations. Groundwater commonly includes cations such as Ca^{2+}, Mg^{2+}, Na^{+}, and K^{+} which could each impact fines migration and immobilization differently. In the case of low or high salinity injections, fluid chemistry of the injection solution should likely be closely considered in relation to the geochemistry of the natural environment. Further work needs to be done to identify the reversibility of these reactions and the permanence of immobilization.

Acknowledgements

The experimental system used for column and imaging experiments was supported by the National Science Foundation under Grant No. 2002412. Any opinions, findings, and conclusions or recommendations expressed in this material are those of the author(s) and do not necessarily reflect the views of the National Science Foundation. Additional support for this work was provided by the Office of the Vice Chancellor for Research and Graduate Education at the University of Wisconsin-Madison with funding from the Wisconsin Alumni Research Foundation.

Nomenclature

CFT	Colloid Filtration Thoery
DLVO	Derjaguin, Landau, Verwey, and Overbeek theory
pH	Potential of Hydrogen
PET	Positron Emission Tomography
mM	milliMolar
PIPES	Piperazine-1,4-bis (2-ethanesulfonic acid) sesquisodium salt
NaOH	Sodium Hydroxide
$^{64}Cu^{2+}$	$^{64}Copper^{2+}$
DI	Deionized
µL	Microliter
M	Molar
mCi/mL	Microcurie per Milliliter
g	grams
PEEK	Polyetheretherketone
mL/min	Milliliter per Minute
ADE	Advection Dispersion Equation
C	Concentration
t	Time
v	Pore Water Velocity
D	Dispersion Coefficient
D_e	Diffusion Coefficient
α_L	Longitudinal Advection
C_a	Solute or Colloid Concentration
K	First Order Attachment or Detachment Coefficient
η	Total Forces Described by Colloid Filtration Theory
ϕ	Porosity
d_c	Diameter of Collector Grain
α	Attachment Term
μm	Micrometer
V_{DLVO}	Total Summation of DLVO Forces
V_{LDW}	van der Waals Forces
V_{EDL}	Electrical Double Layer Forces
V_{BR}	Born Repulsion Forces
cm	Centimeter
^{18}F	Fluorine 18
[^{18}F]FDG	Fludeoxyglucose Fluorine 18
nm	nanometer
Ca^{2+}	Calcium
Mg^{2+}	Magnesium
K^{+}	Potassium

References

1. C. Shen, B. Li, Y. Huang, Y. Jin, Environ. Sci. Technol. 41 (2007)
2. A. Busch, P. Bertier, Y. Gensterblum, Geomech. Geophys. Geo-energ. Geo-resour. 2 (2016)
3. S.G. Sarkisyan, Sed. Geol. 7, 1 (1972)
4. MIT, The Future of Natural Gas – An Interdisciplinary MIT Study, MIT, (2011)
5. H.H. Murray, Dev. Clay Sci. 2 (2006)
6. S.F. Kia, H. S. Fogler, M.G. Reed, R.N. Vaidya, SPE Prod Eng 2, 04 (1987)
7. F. Civan, Gulf Pro. Pub. (2007)
8. T. Russel, D. Pham, M.T. Neishaboor, A. Badalyan, A. Behr, L. Genolet, P. Kowollik, A. Zeinijahromi, P. Bedrikovetsky, J. Nat. Gas Sci. Eng. 45 (2017)
9. K.M. Yao, M.T. Habibian, C.R. O'Melia, Environ. Sci. Technol. 5 (1971)
10. S. Sasidharan, S. A. Bradford, S. Torkzaban, X. Ye, J. Vanderzalm, X. Du, D. Page, Sci. Total Environ. 603–604 (2017)
11. B.V. Derjaguin, LD. Landau, Acta Phys. Chim. 15 (1943)
12. E.J.W. Verwey, J.Th.G. Overbeek, J. Phys. Chem, 51, 3 (1947)
13. J.A. Redman, S.L. Walker, M. Elimelech, Envi-ron. Sci. Technol. 38 (2004)
14. R. Muneer, M.R. Hashmet, P. Pourafshary, ACS omega. 5, 49 (2020)
15. S. Tangparitkul, A. Saul, C. Leelasukseree, M. Yusuf, A. Kalantariasl, J. Pet. Sci. Eng., 194 (2020)
16. R.N. Vaidya, H.S. Fogler, Col Surf. 50 (1990)
17. K. M. Ahmad, F. Kristaly, Z. Turzo, R. Docs, J Oil Gas Petrochem Sci. 1, 1 (2018)
18. P. Schindler, P. Liechti, J. Westall, J. Colloid Interface Sci. 35, 3 (1987)
19. E. Wieland, W. Stumm, Geochim Cosmochim Aca 59, 9 (1992)
20. A. Ferris, W. Jepson, J. Colloid Interface Sci. 51, 2 (1975)
21. M. Kosmulski, Adv. Colloid Interface Sci. 275 (2020)
22. S.A. Bradford, S. Torkzaban, H. Kim, J. Simunek, Water Resour. Res. 48 (2012)
23. Q. Yu, A. Kandegedara, Y. Xu, D.B. Rorabacher, Anal. Bioch. 253, 1 (1997)
24. P.W. Schindler, P. Liechti, J. C. Westall, J. Ag. Sci. 35 (1987)
25. M. Alkan, B. Kalay, M. Dogan, O. Demirbas, J. Hazard. Mater. 153 (2008)
26. M.Q. Jiang, X.Y. Jin, X.Q. Lu, Z.L. Chen, Desalination 252 (2010)
27. R. Chakravarty, S. Chakraborty, A. Dash, Mol. Pharm. 13 (2016) 10.1021/acs.molpharmaceut.6b00582
28. B. Gutfilen, S. AL Souza, G. Valentini, Drug Des. Dev. Ther. 12 (2018)

29. W. Roy, I.Krapac, S. Chou, R. Griffin, U.S. E.P.A., EPA/530/SW-87/006F (2004)
30. C. Zahasky, T. Kurotori, R. Pini, S.M. Benson, Adv. Water Res. 127 (2019)
31. M. van Genuchten, W.J. Alves, U.S.D.A. Tech. Bul. 1661 (1982)
32. J.C. Parker, M. van Genuchten, W. R. Res. 20, 7 (1984)
33. X. Li, T.D. Scheibe, W.P. Johnson, Env. Sci. Tech. 38 (2004)
34. L. Chequer, P. Bedrikovetsky, T. Carageorgos, A. Badalyan, V. Gitis, W. R. Res. 55, 7 (2019)
35. S.A. Bradford, H. Kim, J Environ Qual. 39, (6) (2010) doi: 10.2134/jeq2010.0156. PMID: 21284301
36. C. Zahasky, S.M. Benson, Adv. Water Res. 115 (2018)
37. T. Kurotori, C. Zahasky, S.A.H. Hejazi, S.M. Shah, S.M. Benson, Chem. Eng. Sci. 196 (2019)
38. A. Al-Sarihi, T. Russell, P. Bedrikovetsky, A. Zeinijahromi, Ener. Fuel. 33 (2019)